Deflection and diffraction of x rays bound to curved surfaces

Chien Liu

Division of Engineering and Applied Sciences, Harvard University, Cambridge, Massachusetts 02138, and Rowland Institute for Science, Cambridge, Massachusetts 02142

Jene A. Golovchenko

Division of Engineering and Applied Sciences and Department of Physics, Harvard University, Cambridge, Massachusetts 02138, and Rowland Institute for Science, Cambridge, Massachusetts 02142

Received January 4, 1999

We present two new x-ray optical effects observed on a whispering-gallery waveguide. The first is a gradual in-surface deflection of guided waves caused by the non-Euclidean intrinsic curvature of the waveguide surface. The second is the excitation of in-surface dynamical diffraction modes that reflects the strong influence of the surface photonic band structure of a crystalline waveguide. Both phenomena portend a rich array of basic and applied x-ray optical potentialities. © 1999 Optical Society of America

OCIS codes: 230.7370, 340.0340, 050.1940, 240.0240.

The rapid development of ever-more intense and ultrafast x-ray sources from synchrotrons and near-surface laser–plasma interactions creates opportunities to explore new optical manifestations of the interaction of radiation and matter. Recently, short-wavelength (<0.1-nm) x-ray propagation over great distances along curved surfaces was observed[1] that is the optical couterpart of the (acoustic) whispering-gallery (WG) effect explained by Lord Rayleigh more than a century ago.[2] In the soft-x-ray regime there has been much theoretical and some experimental work in exploring the possibility of using the WG effect to achieve focusing, deflection, and circular polarization of x rays, and even the construction of resonant cavities for laser operation.[3] Here we show two new phenomena connected with surface-bound WG x-ray modes. The first is a gradual in-surface deflection of x-ray paths induced by the intrinsic curvature of the surface. It is related to the deflection of light induced by the gravitational distortion of space–time, but here it is the non-Euclidean nature of the binding surface that creates the force on the photons. The second phenomenon is the excitation of strong in-surface diffraction modes caused by atomic-scale periodicity in a curved crystal waveguide. This diffraction is of interest in its own right and will also prove crucial for demonstrating the gradual ray deflection mentioned above. The diffraction modes display strong dynamical effects reflecting the photonic band structure[4] of the surface that influence absorption and Poynting-vector-controlled energy flow.

The WG x-ray modes are waves gliding along a curved surface.[1] They reside mainly on the vacuum side of the guiding surface. Figure 1 depicts the shape of a bent silicon crystal that was used as an x-ray waveguide. The crystal orientation relative to the incident x-ray beam is also indicated. A triangular-shaped sample is used because a displacement of a corner relative to its clamped opposite side results in a waveguide with a nearly constant radius of curvature R. The 100-μm-thick 2-cm-long waveguide is chemically prepared[5] to terminate the silicon (111) surface bonds with hydrogen. Enclosing the waveguide in a helium bag during the experiment reduces surface contamination. The waveguide is bent horizontally, and we monitor the adjustable radius of curvature by reflecting a laser beam from its surface.

Our observation of in-surface deflection induced by intrinsic curvature relied on uncovering the in-surface diffraction modes first. We used beamline X-15A at the National Synchrotron Light Source at Brookhaven National Laboratory. The beam was prepared by a double-crystal monochromator[6] consisting of a symmetrically and an asymmetrically cut Si(220) crystal. The resulting 17.5-keV x rays were collimated to a 40-μm-wide by 3-mm-high beam before being coupled into the waveguide. The incident x-ray beam formed an angle θ with the $(\bar{2}20)$ lattice planes (which are normal to the surface) and a grazing angle φ relative to the (111) surface (Fig. 1). The monochromator limited the vertical divergence ($\delta\theta$) to 1.56 μrad. The slits and the synchrotron source size limited the horizontal divergence ($\delta\varphi$) to 0.05 mrad. At each bending position of the waveguide the angle θ was scanned through the (220) Bragg angle θ_B with the grazing angle φ fixed, and the exiting guided and diffracted beams were monitored by two collimated NaI detectors or recorded on film.

Figures 2(a)–2(c) shows three film exposures and the corresponding schematic beam paths at different

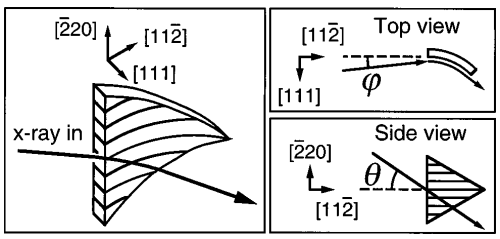

Fig. 1. Relative orientations of an incident x-ray beam and a bent Si(111) waveguide. Parallel curves indicate $(\bar{2}20)$ lattice planes. The synchrotron radiation **E** field is horizontal, normal to the waveguide surface, and parallel to the $(\bar{2}20)$ lattice planes.

0146-9592/99/090587-03$15.00/0

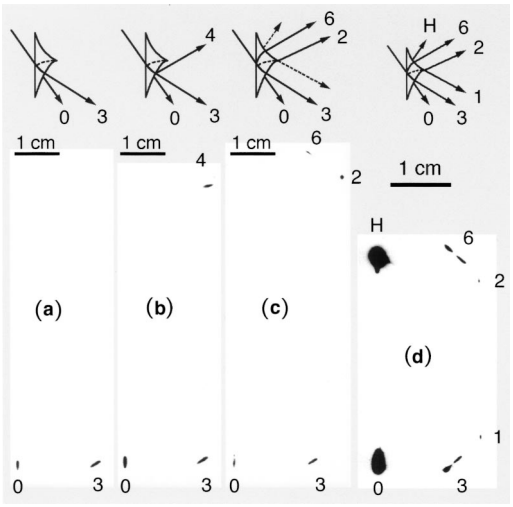

Fig. 2. Schematic beam-path and film exposures taken at (a) $\theta - \theta_B = 1.745$ mrad, (b) $\theta - \theta_B = -0.122$ mrad, and (c) $\theta - \theta_B = 0$ mrad for 17.5-keV x rays on a $R = 15$ cm Si(111) waveguide with grazing angle $\varphi = 0.5$ mrad. (d) $\theta = \theta_B$, $R = 10$ cm, $\varphi = 0.75$ mrad.

stages of a θ scan. The film was placed 162 mm from the entrance of the waveguide, perpendicular to the incident beam. The waveguide radius of curvature was $R = 15$ cm, and the grazing angle φ, 0.5 mrad. The straight-through beam (footprint 0) is present in all pictures. Far from the Bragg condition [Fig. 2(a), $\theta - \theta_B = 1.745$ mrad], only nondiffracting WG modes are excited. These modes glide along the horizontally bent surface, leading to the horizontally displaced exit beam (footprint 3). Near but distinctly displaced from the Bragg condition [Fig. 2(b), $\theta - \theta_B = -0.122$ mrad], a strong diffracted ray appears at footprint 4. Tracing this ray back to the waveguide shows that it corresponds to WG modes that are diffracted near the exit edge. These modes follow the horizontally curved surface nearly all the way across the waveguide before being diffracted vertically. Curiously, this edge-diffracted beam disappears in the Bragg condition [Fig. 2(c), $\theta = \theta_B$].

At $\theta = \theta_B$ two spatially separate diffraction peaks appear instead at footprints 6 and 2. The first is diffracted vertically near the front of the waveguide and then coupled into nondiffracting WG modes. Footprint 2 is traced back to the tip of the waveguide and is shown below to correspond to a strongly diffracting eigenmode of the surface photonic band structure. This picture was taken with slits and absorbers placed between the waveguide and the film to reduce background.

An unblocked picture taken in the Bragg condition is shown in Fig. 2(d). The film was placed 93 mm from the entrance of the waveguide and perpendicular to the $[11\bar{2}]$ reciprocal lattice vector. Here the radius of curvature of the waveguide was $R = 10$ cm, and the grazing angle φ was 0.75 mrad. Footprint H is not a surface effect and corresponds to diffraction of the straight-through beam vertically by the Si bulk. Both footprints 1 and 2 are traced back to the tip of the waveguide, which is entirely inaccessible to x rays if one assumes only kinematic diffraction effects.

A dynamical diffraction theory for trapped x rays on a curved crystal surface should be consistent with the intuitive observation that the evanescent tails of WG modes can interact with the underlying crystal lattice, resulting in strong diffraction effects.[7] We solve the Maxwell equations in the cylindrical coordinates (ρ, ϕ, z) for a waveguide surface with radius R and reciprocal lattice vector $\mathbf{H} = H \cdot \hat{z}$. The dielectric function is 1 for $\rho < R$ and $1 - \delta_0 - \delta_H[\exp(iHz) + \exp(-iHz)]$ for $\rho > R$, where $1 - \delta_0$ gives the average value of the dielectric constant and δ_H is its Fourier component for reciprocal lattice vector $\mathbf{H}$. The eigenfunction in the photonic bandgap region is composed of a forward and a diffracted wave,

$$\mathbf{E}_{\nu, k_{z_0}}(\rho, \phi, z, t) \equiv [\mathbf{E}_0(\rho)\exp(ik_{z_0}z) + \mathbf{E}_H(\rho)\exp(ik_{z_H}z)]\exp(i\nu\phi - i\omega t), \quad (1)$$

where $k_{z_H} \equiv k_{z_0} + H$, with a similar form for the $\mathbf{B}$ field. The eigensolutions to the Maxwell equations are dynamically diffracting WG modes traveling in the $\hat{\phi}$ direction and bound radially near the crystal surface, with an evanescent tail penetrating into the waveguide. In the $\hat{z}$ direction the interference of the two plane-wave components results in a complete or a partial standing wave, depending on the polarization and the magnitude of the z wave-vector components k_{z_0} and k_{z_H}. The theory predicts that the attenuation along the surface (in the $\hat{\phi}$ direction) of the various eigensolutions can differ dramatically from expectations based on theory for the bulk.[8]

The origin of the footprints 1 and 2 in Fig. 2(d) can now be understood. Once the incident x ray is coupled into the dynamically diffracted WG modes, they propagate with the Poynting vector along the lattice planes toward the tip of the waveguide, where the forward and the diffracted components emerge and are decoupled to plane waves, which reach the film at footprints 1 and 2, respectively. These footprints would not exist if full nonperturbative eigenmodes of the surface photonic band structure were not excited.

In-surface deflection of an x-ray path caused by the intrinsic curvature of the waveguide is revealed by use of the dynamical diffraction angular condition to reference the angular change of the x-ray direction for an in-surface curved path. In Figs. 2(b) and 2(c), a kinematic exit-edge diffraction peak occurs displaced 0.122 mrad away from the Bragg angle at which the dynamical diffraction occurs. The displaced peak is due to the gradual angular deflection (relative to the diffracting planes) of an undiffracted surface mode propagating up to the exit edge of the waveguide, where the diffraction condition is finally satisfied. The angular separation $\Delta\theta$ between the two diffraction peaks can be read from a θ scan, as shown in the inset of Fig. 3(c).

The geometry of a model that quantitatively accounts for $\Delta\theta$ is depicted in Figs. 3(a) and 3(b), which show the propagation of WG x rays on a two-dimensionally distorted rectangular Si(111) plate

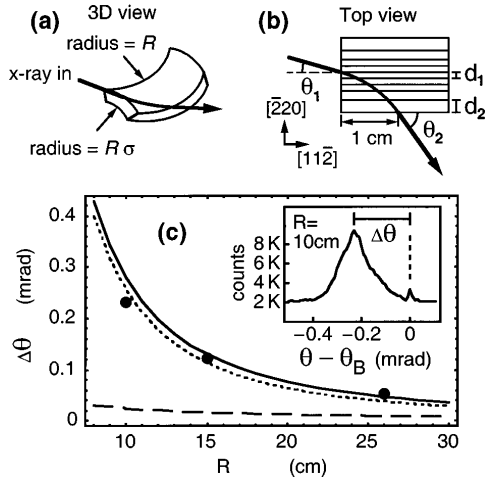

Fig. 3. (a) and (b) X-ray path on a bent Si plate with a saddlelike surface and a relaxed lattice. (c) Inset, θ scan showing the dynamic diffraction peak at $\theta = \theta_B$ and the edge diffraction peak at $\theta - \theta_B = -0.231$ mrad for 17.5-keV WG x-rays on a $R = 10$ cm Si(111) waveguide. The graph shows the angular separation of the two peaks, $\Delta\theta \equiv |\theta - \theta_B|$, as a function of R.

of thickness t. A bend of the plate of a radius of curvature R in the $[11\bar{2}]$ direction will be accompanied by a bend with radius of curvature $-R\sigma$ in the $[\bar{2}20]$ direction, where $\sigma = 3.82$ is the Poisson ratio.[9,10] This second bend introduces two effects that contribute to $\Delta\theta$. The first is the gradual in-surface deflection of the x-ray path. The curvatures in the $[11\bar{2}]$ and $[\bar{2}20]$ directions render the crystal surface saddlelike [Fig. 3(a)]. The optical path, selected by Fermat's principle, is curved and is schematically depicted in Fig. 3(b). The difference in the angle of the WG x-ray beam relative to the crystal orientation, $\theta_2 - \theta_1$, directly contributes to $\Delta\theta$. A calculation of this contribution is shown as a dotted curve in Fig. 3(c). The second contribution to $\Delta\theta$ is from a change in the surface-lattice constant. In general, for a bent plate, most of the surface-stress relaxation is concentrated near the edges.[11] The percentage difference in lattice constants between the center and the edge of the plate [Fig. 3(b)] is given by $d_2/d_1 - 1 = t/(2R\sigma)$, leading to a change in the local Bragg angle. This small contribution is shown as the dashed curve in Fig. 3(c). The total contribution is shown as the solid curve in Fig. 3(c). It agrees remarkably well with the experimental values.

The diffraction and deflection of WG x rays exhibit a rich array of wave-propagation phenomena. Even more spectacular effects of intrinsic surface curvature are expected in the spatial propagation of dynamically diffracted surface eigenmodes. Structures with specially engineered surface curvature and periodicity may one day be used to manipulate x-ray beams in very intricate ways. Potential applications include resonant cavities for x-ray lasers, optical elements for x-ray interferometers, microscopes and lithography, and the study of thin, specially prepared two-dimensional surface layers of interest in materials science and biology.[12] The capture of x rays from near-surface laser–plasma interactions in WG modes whose spatial extent outside (inside) the surface can be reduced to less than 100 nm (5 nm) should provide valuable insight into the spatial–temporal properties of the picosecond-to-subpicosecond x rays produced by this method.[13] We also hope that the x-ray phenomena that we have discussed here will stimulate analogous studies at optical wavelengths in artificially prepared periodic media.

We thank P. F. Lyman, T.-L. Lee, and M. M. Burns for their help. This work was supported by the Harvard Materials Research Science and Engineering Center (contract NSF-DMR-8920490).

References

1. Chien Liu and J. A. Golovchenko, Phys. Rev. Lett. **79,** 788 (1997).
2. Lord Rayleigh, *The Theory of Sound*, American ed. (Dover, New York, 1945).
3. J. P. Braud and P. L. Hagelstein, IEEE J. Quantum Electron. **27,** 1069 (1991); N. V. Smith and M. R. Howells, Nucl. Instrum. Methods Phys. Res. A **347,** 115 (1994); I. N. Bukreva, I. V. Kozhevnikov, and A. V. Vinogradov, Proc. SPIE **2453,** 80 (1995).
4. J. D. Joannopoulos, R. D. Meade, and J. N. Winn, *Photonic Crystals* (Princeton U. Press, Princeton, N.J., 1995).
5. A. Ishizaka and Y. Shiraki, J. Electrochem. Soc. **133,** 666 (1986).
6. R. E. Martinez, "Impurity atoms on a silicon surface: structures, forces and dynamics," Ph.D. dissertation (Harvard University, Cambridge, Mass., 1992); J. A. Golovchenko, R. A. Levesque, and P. L. Cowan, Rev. Sci. Instrum. **52,** 509 (1981).
7. T. Jach, P. L. Cowan, Q. Shen, and M. J. Bedzyk, Phys. Rev. B **39,** 5739 (1989).
8. B. W. Batterman and H. Cole, Rev. Mod. Phys. **36,** 681 (1964).
9. S. P. Timoshenko and J. N. Goodier, *Theory of Elasticity*, 3rd ed. (McGraw-Hill, New York, 1969).
10. R. F. S. Hearmon, *An Introduction to Applied Anisotropic Elasticity* (Oxford University, London, 1961); S. Muramatsu and M. Kitamura, J. Appl. Phys. **73,** 4270 (1993).
11. F. A. McClintock and A. S. Argon, eds., *Mechanical Behavior of Materials* (Addison-Wesley, Reading, 1966), p. 349.
12. C. Rischel, A. Rousse, I. Uschmann, P.-A. Albouy, J.-P. Geindre, P. Audebert, J.-C. Gauthier, E. Forster, J.-L. Martin, and A. Antonetti, Nature (London) **390,** 490 (1997).
13. M. M. Murnane, H. C. Kapteyn, M. D. Rosen, and R. W. Falcone, Science **251,** 531 (1991).